Hybrid paramagnon phonon modes at elevated temperatures in EuTiO3

Bussmann-Holder, A ; Guguchia, Z ; Köhler, J ; Keller, H ; Shengelaya, A ; Bishop, A R

DOI: https://doi.org/10.1088/1367-2630/14/9/093013

Hybrid paramagnon phonon modes at elevated temperatures in $EuTiO_3$

2012 New J. Phys. 14 093013

(http://iopscience.iop.org/1367-2630/14/9/093013)

New Journal of Physics
The open-access journal for physics

Hybrid paramagnon phonon modes at elevated temperatures in $EuTiO_3$

A Bussmann-Holder[1,5], Z Guguchia[2], J Köhler[1], H Keller[2], A Shengelaya[3] and A R Bishop[4]

[1] Max-Planck-Institut für Festkörperforschung, Heisenbergstrasse 1, D-70569 Stuttgart, Germany
[2] Physik Institut der Universität Zürich, Winterthurerstrasse 190, CH-8057 Zürich, Switzerland
[3] Department of Physics, Tbilisi State University, Chavchavadze Avenue 3, GE-0128 Tbilisi, Georgia
[4] Los Alamos National Laboratory, Los Alamos, NM 87545, USA
E-mail: a.bussmann-holder@fkf.mpg.de

New Journal of Physics **14** (2012) 093013 (9pp)
Received 25 May 2012
Published 11 September 2012
Online at http://www.njp.org/
doi:10.1088/1367-2630/14/9/093013

Abstract. $EuTiO_3$ (ETO) has recently experienced a significant revival of interest because of its possible multiferroic properties, which are currently the focus of much research. Unfortunately, ETO is an unlikely candidate for enlarged multifunctionality since the mode softening—typical of ferroelectrics—remains incomplete, and the antiferromagnetic properties appear only at 5.5 K. However, a strong coupling between lattice and Eu spins exists and this leads to the appearance of a magnon–phonon-hybrid mode at elevated temperatures as evidenced by EPR, muon spin relaxation experiments and model predictions based on a coupled spin-polarizability Hamiltonian. This novel finding supports the notion of strong magneto-dielectric effects being realized in ETO and opens up new strategies in material design and technological applications.

ETO is a prototypical cubic perovskite for $T > 300$ K, where the Eu ions occupy the A sublattice in ABO_3, thereby leaving the B-sublattice in the d^0 state which is favorable for ferroelectricity. The low-temperature antiferromagnetic ordering of the Eu spins and their strong coupling to the dielectric properties are clear evidence for a strong spin–lattice interaction [1–5] that is

[5] Author to whom any correspondence should be addressed.

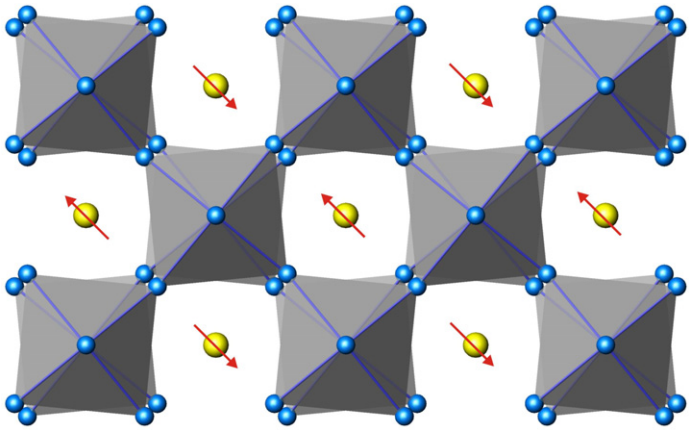

Figure 1. Low-temperature schematic structure of ETO ($T = 100$ K). For clarity the rotation angle has been enlarged by a factor of 2 and the Eu spin order below 5.5 K added. The yellow circles refer to Eu, the blue ones to O and the Ti atoms are centering the octahedron located below the apical oxygen ions.

absent in most ABO_3 compounds. Nevertheless, analogies to these prototypical ferroelectrics remain, especially to $SrTiO_3$ (STO), since Sr and Eu have the same valencies, the same ionic radii and consequently the same lattice constants. In addition, both systems are incipient quantum paraelectrics, which means that the complete mode softening is suppressed by quantum fluctuations [6]. Here, an important difference arises between both because STO has a finite extrapolated ferroelectric transition temperature $T_C = 27$ K, whereas ETO cannot be extrapolated to any finite temperature value, which makes it even less susceptible to ferroelectricity. However, a novel commonality was predicted and experimentally confirmed recently between STO and ETO, namely a rotational instability of the oxygen ion octahedra at $T_S = 282$ K [7, 8]. This zone boundary-related phase transition is analogous to that observed in isostructural STO at $T_S = 105$ K [6, 9, 10]. The refinement of high-resolution x-ray analysis of powder data of ETO in space group I4/mcm taken at $T = 100$ K yielded lattice constants of $a = 5.5192(1)$ Å and $c = 7.8165(1)$ Å [11]. The Eu are in the 4*b* position, Ti in 4*c*, O1 in 4*a* and O2 in 8*h* with $x = 0.238(1)$, see figure 1.

In analogy to STO this phase transition has been related to the softening of a transverse zone boundary acoustic mode frequency, which is predicted to display a very similar [7, 8] temperature dependence as observed in STO and reminiscent of a purely displacive transition. However, the calculations indicate that the related double-well potentials differ grossly; STO has a broad and shallow double-well potential, whereas ETO exhibits a deep and narrow one [12]. The crossover in the dynamics between these two extremes was demonstrated by investigating the phase diagram of the mixed crystal series $Sr_{1-x}Eu_xTiO_3$, where a nonlinear dependence of T_S on x was observed [12].

Here, we concentrate on the pure ETO system and investigate its magnetic properties in relation to the soft mode dynamics. Motivated by the strong spin–phonon coupling observed at the onset of AFM order, similar strong interactions are expected to appear at the structural phase transition for the following reasons: from first-principles GGA + U calculations [8] it appeared that two competing spin–spin interactions between nearest- and second-nearest-neighbor 4f spins ($S = 7/2$) are present in ETO, namely the nearest-neighbor AFM interaction J_{nn} and

the second-nearest-neighbor ferromagnetic interaction J_{nnn}. Both are almost of the same order of magnitude. While J_{nn} should be unaffected by the oxygen octahedral rotation, J_{nnn} varies with it, since this is the indirect one via the bridging (and rotating) oxygen ion. This suggests that J_{nnn} adopts a temperature dependence analogous to the soft zone boundary mode. In addition, correlated spin fluctuations appear, which are evidenced by muon spin relaxation (μSR) techniques.

The system is modeled within a spin–phonon coupled approach [7, 8, 13] with the phonon subsystem described by the nonlinear polarizability model [14–16]. This guarantees that the optic mode softening is correctly reproduced and allows a self-consistent derivation of the local double-well potential [8, 12]. In addition, predictions on the zone boundary acoustic mode softening have been made [12]. The essential ingredients of the model are the nonlinear polarizability of the oxygen ion O^{2-}, which is unstable as a free ion and partially stabilized by the Madelung potential of the surrounding lattice [17]. This property is modeled by an attractive harmonic core–shell coupling g_2 and an anharmonic fourth-order coupling g_4 in the relative core–shell displacement coordinate w where both quantities have to be derived self-consistently. The stability of the system is guaranteed by a second-nearest-neighbor harmonic coupling f' between the polarizable units. The nearest-neighbor coupling f between the rigid ion sublattice and the polarizable units together with the core–shell coupling $g_T = g_2 + 3g_4\langle w^2\rangle_T$ ensures mode–mode coupling and produces anomalies in the elastic constants. The coupling between the spins and the lattice, ε, modifies, through the lattice dynamics, the xy components of the g tensors, whereby ε varies linearly with the magnetic field H. The dispersion relations for the coupled mode system have been derived in [7, 8].

For small spin–lattice coupling, the zero momentum optic mode softens with decreasing temperature. In this limit the soft optic mode has the same temperature dependence as in the uncoupled case. For increasing spin–phonon coupling, respectively increasing field strengths, $\varepsilon \approx H$, the soft mode frequency hardens with increasing coupling in agreement with experimental data [1–3]. In addition, the mean value of the z-component of the spin is affected and will depress the dielectric constant differently for fields parallel or perpendicular to it. Besides the anomalous low-temperature behavior of the dielectric constant, a strong coupling of the Eu spins with the optic and acoustic branch sets in with finite ε, which modifies the dispersion of all modes and admits for short-range magnetic order above T_{N}, namely already in the paramagnetic phase. The theoretical situation for different magnon energies ω_0 and with momentum q along (100) where the soft optic mode is observed is shown in figure 2 as a function of temperature.

With decreasing temperature, an increased magneto-acoustic coupling sets in for both magnon and phonon energies, which leads to a substantial suppression of the acoustic mode for large magnon energies (figure 2(a)) at the zone boundary. This acoustic–paramagnon coupling should also be evident in the piezo-magnetic response. The optic mode is not affected by the spin mode at the zone boundary where it adopts its rigid ion value. However, at small momentum the optic mode softening gets pinned at the magnon energy with decreasing temperature and a polar instability is inhibited. Finite momentum optic mode magnon coupling exists for $q < 0.2$ with the wave vector providing information on the real space spin modulations. For $q \approx 0.2$, this corresponds to roughly five lattice constants. A rather similar paramagnon–phonon coupling to that described above has been observed in hexagonal $YMnO_3$ [17, 18], where 10 K above the magnetic ordering temperature a spin wave mode has been observed which strongly interacts with the optic and acoustic phonon mode branches.

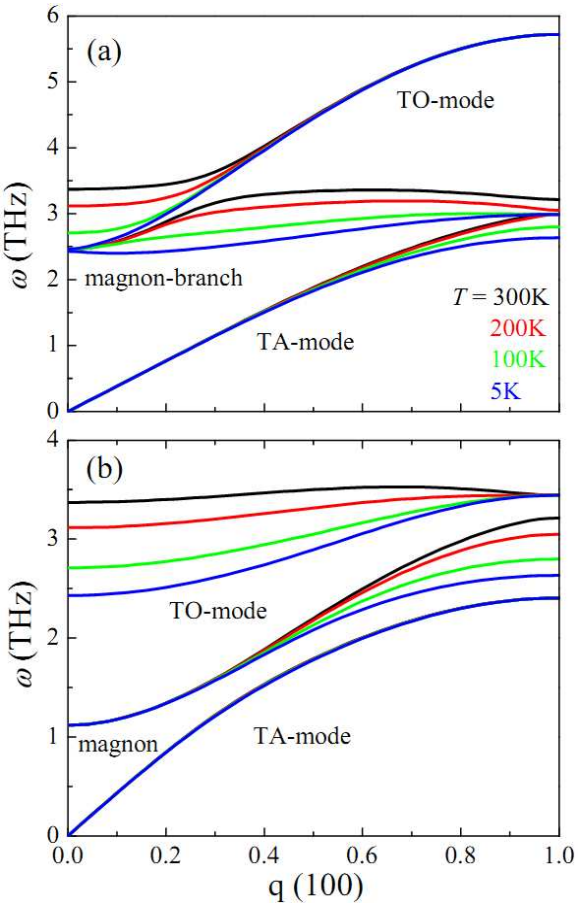

Figure 2. Temperature dependence of the dispersion of the magnon and optic and acoustic mode frequencies for (a) magnon with energy $\omega_0 = 2.5$ THz and (b) $\omega_0 = 1.2$ THz. The temperatures are given by the color code shown in the figure. The calculations refer to momentum q along (100).

Such a coupling is reminiscent of the hybridized soft mode of $TbMnO_3$ [19] observed by inelastic neutron scattering. It depends, however, on the value of the paramagnon energy ω_0.

For small values of ω_0 (figure 2(b)), a crossing of magnon and acoustic branches takes place at small momentum, leading to pronounced magneto-electric coupling. The latter evolution with temperature has been reported in [20] for hexagonal $YMnO_3$ where far above the Néel temperature short-range magnetic correlations enable the observation of phonon–paramagnon coupling, rather analogous to the above results. In this case the long-wavelength optic mode softens similarly to the uncoupled case. At intermediate momentum values, however, the softening remains and is attributed to another crossing of the magnon branch with the optic mode.

The predicted finite-size phonon–paramagnon coupling at temperatures $T > T_N$, T_S has been tested experimentally by μSR spectroscopy measurements. Zero-field (ZF) μSR experiments were performed at the μE1 and πM3 beam lines of the Paul Scherrer Institute (Villigen, Switzerland). The polycrystalline ETO sample has been prepared as described in [7]. The sample was mounted on a sample holder with a standard veto setup providing essentially a low-background μSR signal.

In a μSR experiment nearly 100% spin-polarized muons are implanted into the sample one at a time. The positively charged muons μ^+ thermalize at interstitial lattice sites, where they act as magnetic microprobes. In a magnetic material, the muon spin precesses in the local magnetic field B_μ at the muon site with the Larmor frequency $\nu_\mu = \gamma_\mu/(2\pi)B_\mu$ (muon gyromagnetic ratio $\gamma_\mu/(2\pi) = 135.5\,\mathrm{MHz\,T^{-1}}$). ZF-$\mu$SR is a very powerful tool to investigate microscopic magnetic properties of solids without applying an external magnetic field. A ZF-μSR time spectrum for the polycrystalline ETO sample recorded at 1.6 K is shown in the inset of figure 1(A). At this temperature a spontaneous muon spin precession is observed, indicating a well-defined internal magnetic field at the muon sites, consistent with the low-temperature AFM phase stemming from the ordering of the 4f spins of Eu with total spin $S = 7/2$. The ZF-μSR data below T_N are analyzed using the functional form $\mathrm{A(t)} = A_\mathrm{s}(t) + A_\mathrm{BG}(t)$ with the first component describing the sample response and the second one representing the background contribution. The sample contribution is described by the expression

$$A_\mathrm{s}(t) = A_0\left[\frac{2}{3}\exp\left(-\lambda_T t\right)\cos(\gamma_\mu B_\mu t + \phi) + \frac{1}{3}\exp\left(-\lambda_L t\right)\right]$$

where A_0 denotes the initial asymmetry, and φ is the initial phase of the muon–spin ensemble. B_μ represents the internal magnetic field at the muon site, and the depolarization rates λ_T and λ_L characterize the damping of the oscillating and non-oscillating parts of the μSR signal. The two-third oscillating and the one-third non-oscillating μSR signal fractions originate from the spatial averaging in powder samples, where two-thirds of the magnetic field components are perpendicular to the muon spin and cause a precession, while one-third of the field components are parallel and do not contribute. Using the analysis described in detail above, the low-temperature part of the μSR rate is displayed in the inset to figure 3(a), which vanishes—as expected—at T_N. The internal field B_μ is given in the main part of figure 3(a). In figure 3(b) the relaxation rates λ_L and λ_T are shown as a function of temperature. The transition to the AFM state is marked by a divergence in λ_L and a peak in λ_T (critical slowing down) upon approaching T_N.

The above data evidence that our method is very sensitive in detecting any kind of magnetic order in ETO.

For temperature $T > T_\mathrm{N}$ the oscillatory time evolution of the asymmetry vanishes, but still a damped decay rate of $A(t)$ remains, stemming from thermally induced magnetic disorder of randomly oriented spins. In this temperature range the analysis becomes statistically compatible with the single exponential component $A(t) = A_0\exp\left(-\lambda_\mathrm{para}t\right)$, with A_0 denoting the initial asymmetry and λ_para is the relaxation rate referring to the magnetic moments surrounding the muon. The temperature dependence of the relaxation rate λ_para of polycrystalline ETO in the paramagnetic phase is shown in figure 4(a). At the structural transition T_S a pronounced anomaly in $\lambda_\mathrm{para}(T)$ is observed, demonstrating that at T_S the magnetic moments, surrounding the muon spin, change due to a change in the structure. As has been outlined above, two competing interactions between the spins exist, the nearest-neighbor AFM exchange J_nn and the next-nearest-neighbor ferromagnetic superexchange J_nnn via the in between lying oxygen ions. Both interactions are closely balanced [8]. Since at T_S the oxygen ion octahedra rotate anticlockwise with respect to each other [11], J_nnn is altered at T_S and induces a change in the μSR rate caused by pronounced spin–lattice interaction. This survives even above the structural transition temperature. We demonstrate this conclusion by comparing the temperature dependence of λ_para

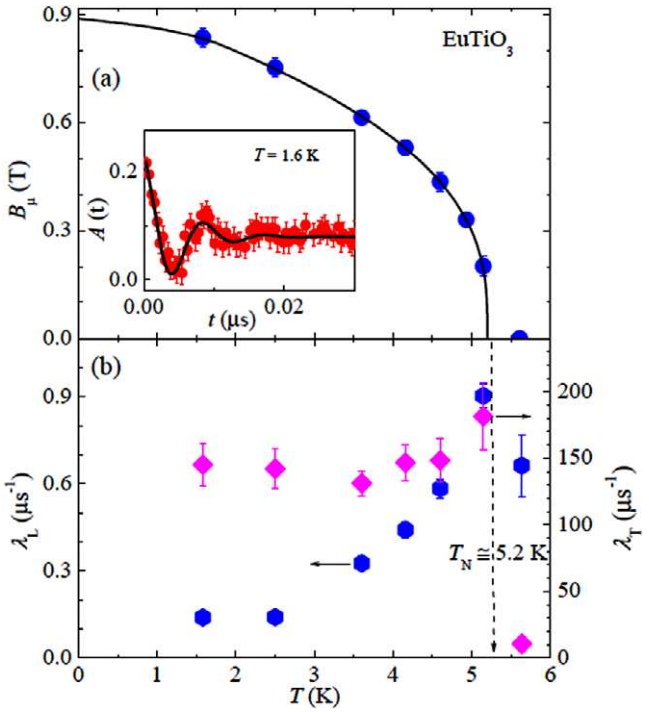

Figure 3. (a) Temperature dependence of the internal field B_μ of polycrystalline ETO. The inset to figure 3(a) shows the ZF-μSR spectrum of polycrystalline ETO below T_N at $T = 1.6$ K. (b) Temperature dependence of λ_L andλ_T.

with that of the zone boundary soft mode frequency and the EPR line width of [12] (figures 4(b) and (c)), already presented in [12]. In contrast to [12] we have plotted the squared frequency $\omega_{TA}^2(q = 2\pi/a)$ as a function of $(T - T_S)$ and applied the standard mean-field Curie–Weiss law to the mode in the low temperature regime. In order to highlight this analogy further, the mode has been shifted upwards by 3.2 THz^2, but is actually zero at T_S.

While this comparison is not quantified with respect to the direct involvement of the soft zone boundary in the spin dynamics, the similarity between all three temperature dependences is striking and demonstrates that a strong coupling between the spin and the lattice must be present. Also, it is important to note that the soft zone boundary mode shows an almost second-order-type phase transition which is accompanied by the slowing down of the relaxation rate at T_S. The analogous temperature dependence of the inverse EPR line width (figure 4(b)) is an additional support for the suggested strong spin–lattice interaction. It is, however, important to point out that both experimental data show fluctuations around T_S which deviate from the mean-field behavior of the soft mode. This small discrepancy can be related to the fact that in the theoretical results fluctuations of the order parameter have not been taken into account even though these might contribute to the dynamics around T_S. A more refined analysis of this regime will be given elsewhere.

The relation between EPR and μSR has been derived in [22]. We follow this analysis closely in the following. The temperature dependence of $1/(\Delta H_{EPR})$ shown in figure 4(b) is similar to $\lambda_{para}(T)$. In order to understand this similarity the relation between $\lambda_{para}(T)$ and the fluctuation time of paramagnetic spins needs to be considered. In [21] the depolarization

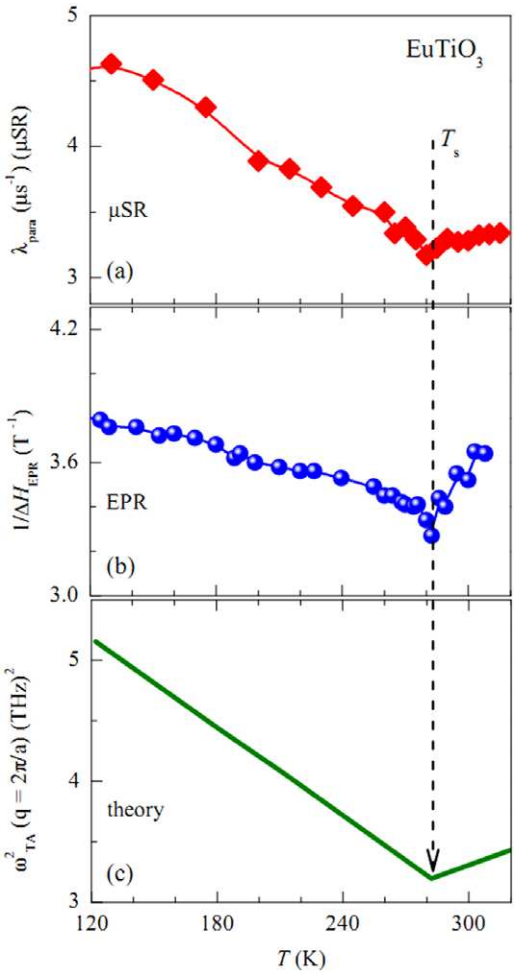

Figure 4. (a) Paramagnetic relaxation rate λ_{para} of polycrystalline ETO as a function of temperature. At the structural transition temperature T_S an anomaly appears which is indicated by an arrow. The solid lines are guides to the eye. (b) The EPR line width of ETO as a function of temperature [12]. (c) Calculated temperature dependence of the squared soft zone boundary transverse acoustic mode $\omega^2_{\text{TA}}(q = 2\pi/a)$ along the projected (111) direction. The mode has been shifted upwards by 3.2 THz^2 in order to illustrate the close analogy with the experimental data.

rate $\lambda_{\text{para}}(T)$ measured in ZF-μSR experiments has been analyzed in the paramagnetic phase of compounds containing 4f-shell ions. It was found that $\lambda_{\text{para}}(T)$ measured at temperatures high with respect to the magnetic phase transition temperature is a function of fluctuation time τ of the 4f spins. In cubic symmetry the $\lambda_{\text{para}}(T)$ can be written as [22] $\lambda_{\text{para}}(T) = 2\Delta_e^2\tau(T)$, where Δ_e is the hyperfine coupling constant between the muon spin and the localized 4f moments. From EPR it was observed that the dominant contribution to the relaxation mechanism of the 4f ions stems from the spin–phonon coupling. Consequently, the time τ in equation (3A) can be replaced by the spin–lattice relaxation (SLR) time T_1. The SLR time is defined by the expression [22] $T_1(s) = 1/(7.62 \times 10^6 g\Delta H_{\text{EPR}})$, which, when combined

with the above relation, yields $\lambda_{\text{para}}(T) = 2\Delta_e^2(T)/(7.62 \times 10^6 g \Delta H_{\text{EPR}})$. This agrees well with the experimentally observed correlation between $\lambda_{\text{para}}(T)$ and $1/(\Delta H_{\text{EPR}})$.

Since it is well known that the actual spin ordering temperature is $T_N = 5.5$ K, we conclude from the data and the theoretical analysis that the Eu spins follow the lattice dynamics within spatially limited regions, i.e. short-range structural order. They are dragged by the mode softening and fluctuate locally in an ordered manner, thus giving rise to the μSR response at elevated temperatures. This finite-size coupling between the spins and the optic and acoustic mode branches is expected to give rise to novel piezo-magnetic, opto-magnetic and magneto-elastic effects. Since the spin ordering is not coherent on the lattice the system represents an inherently inhomogeneous state with locally confined dynamical interactions underlining our conclusion about the strong hybrid paramagnon–phonon coupling.

Acknowledgments

The experiment was performed at the Swiss Muon Source, Paul Scherrer Institute (PSI), Villigen, Switzerland. The μSR time spectra have been analyzed using the free software package musrfit [21] mainly developed by A Suter at PSI. We thank A Amato, Z Shermadini and A Maisuradze for their support during the μSR experiments. This work was partly supported by the Swiss National Science Foundation and the SCOPES grant no. IZ73Z0_128242.

References

[1] Katsufuji T and Takagi H 2001 *Phys. Rev.* B **64** 054415
[2] McGuire T R, Shafer M W, Joenk R J, Halperin H A and Pickart S J 1966 *J. Appl. Phys.* **37** 981
[3] Kamba S, Nuzhnyy D, Vaněk P, Savinov M, Knížek K, Shen Z, Šantavá E, Maca K, Sadowski M and Petzelt J 2007 *Europhys. Lett.* **80** 27002
[4] Goian V, Kamba S, Hlinka J, Vaněk P, Belik A A, Kolodiazhnyi T and Petzelt J 2009 *Eur. Phys. J.* B **71** 429
[5] Goian V, Kamba S, Nuzhnyy D, Vaněk P, Kempa M, Bovtun V, Knížek K, Prokleška J, Borodavka F, Ledinský M and Gregora I 2011 *J. Phys.: Condens. Matter* **23** 025904
[6] Müller K A and Burkhard H 1979 *Phys. Rev.* B **19** 3593
[7] Bussmann-Holder A, Köhler J, Kremer R K and Law J M 2011 *Phys. Rev.* B **83** 212102
[8] Bettis J L, Whangbo M H, Köhler J, Bussmann-Holder A and Bishop A R 2011 *Phys. Rev.* B **84** 184114
[9] Samara G A 2001 Ferroelectricity solid state physics *Advances in Research and Applications* vol 56 (San Diego, CA: Academic) p 240
[10] Cochran W 1960 *Adv. Phys.* **9** 387
Cochran W 1961 *Adv. Phys.* **10** 401
Cochran W 1969 *Adv. Phys.* **18** 157
[11] Köhler J, Dinnebier R and Bussmann-Holder A *Phase Transitions* at press
[12] Guguchia Z, Shengelaya A, Keller H, Köhler J and Bussmann-Holder A 2012 *Phys. Rev.* B **85** 134113
[13] Jacobsen E H and Stephens K W H 1963 *Phys. Rev.* **129** 2036
[14] Migoni R, Bilz H and Bäuerle D 1976 *Phys. Rev. Lett.* **37** 1155
[15] Bilz H, Bussmann A, Bendek G and Strauch D 1980 *Ferroelectrics* **25** 339
[16] Bilz H, Benedek G and Bussmann-Holder A 1987 *Phys. Rev.* B **35** 4840
[17] Petit S, Moussa F, Pailhès S, Pinsard-Gaudart L and Ivanov A 2007 *Phys. Rev. Lett.* **99** 266604
[18] Chatterji T 2008 *Pramana J. Phys.* **71** 847

[19] Senff D, Link P, Hradil K, Hiess A, Regnault L P, Sidis Y, Aliouane N, Argyriou D N and Braden M 2007 *Phys. Rev. Lett.* **98** 137206

[20] Kadlec C, Goian V, Rushchanskii K Z, Kůzel P, Ležaić M, Kohn K, Pisarev R V and Kamba S 2010 *Phys. Rev.* B **84** 174120

[21] Suter A and Wojek B M 2012 Musrfit: a free platform-independent framework for μSR data analysis *Phys. Procedia* **30** 69–73 (see also http://lmu.web.psi.ch/facilities/software/musrfit/technical/index.html)

[22] Dalmas de Réotier P, Yaouanc A and Bonville P 1996 *J. Phys.: Condens. Matter* **8** 5113